[G³]

Supporting Information for

[Deep free-gas accumulation beneath the Chatham Rise, New Zealand – an AVO study]

[Michael T. Macnaughtan1* Ingo A. Pecher2 Lorna J. Strachan1 Gareth J. Crutchley3]

[1 The School of Environment, The University of Auckland, Auckland, New Zealand.

2 Department of Physical and Natural Sciences. Texas A&M University, Corpus Christi, The United States of America.

3GEOMAR Helmholtz Centre for Ocean Research Kiel, Wischhofstr. Kiel, Germany.]

Contents of this file

Introduction

Text S1 provides information of seafloor amplitudes in both seismic lines used. Text S2 shows AVO inversion wavelets. Text S3 gives detailed observations and interpretation of seismic stratigraphy. Text S4 covers detailed observations of amplitude variations with angle of Sequence Y and MES. Text S5 aims to illustrate the clear background trend identified in seismic stacks. Text S6 highlights the higher gradient attribute values observed in data, which do not represent Base Sequence Y in APB13-06. Text S7 shows Vp/Vs vs P-impedance crossplots, highlighting an interpreted AVO inversion anomaly. Text

S8 shows low porosity Zoeppritz models for two lithologies. Text S9 provides full seismic inversion models produced in this study. Text S10 describes amplitude-based artefacts seen in Figure 2. Text S11 describes the pseudo borehole used during simultaneous inversion.

Text S1.

Figure S1; S2 presents APB13-06 and PEG09-11 seafloor amplitudes, highlighting approximately stable amplitudes along-line.

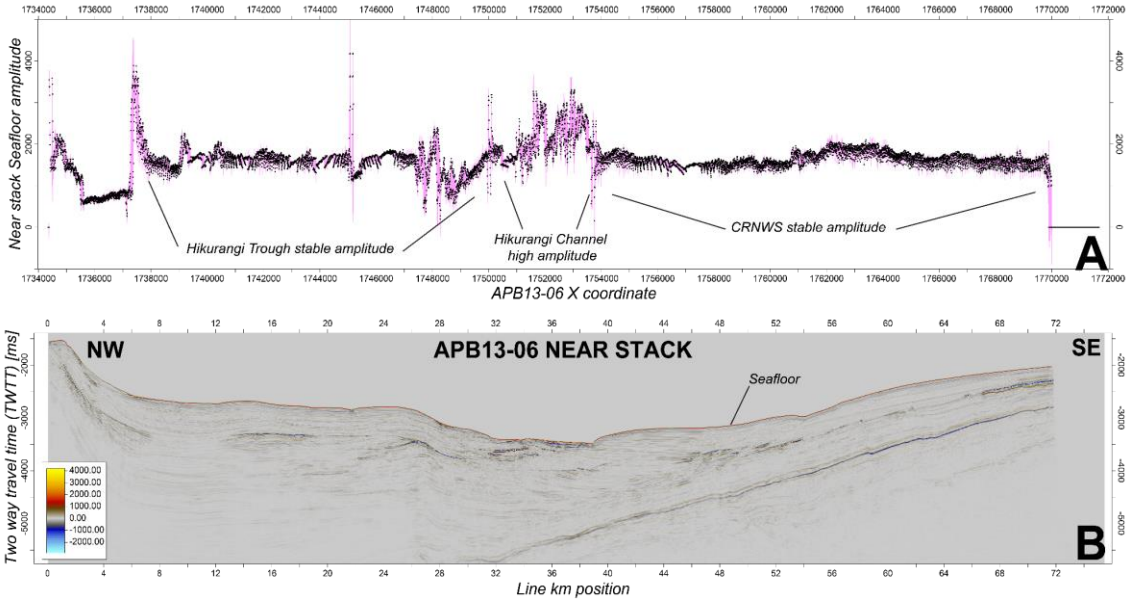

Figure S1. *(A). APB13-06 near stack seafloor amplitudes (black points) plotted against X coordinates. The seafloor X coordinates (meters) are labeled on the X axis. Seafloor*

amplitudes appear stable across the line, increasing only in the Hikurangi Channel (B). APB13-06 Near angle stack, shown in the same scale for reference.

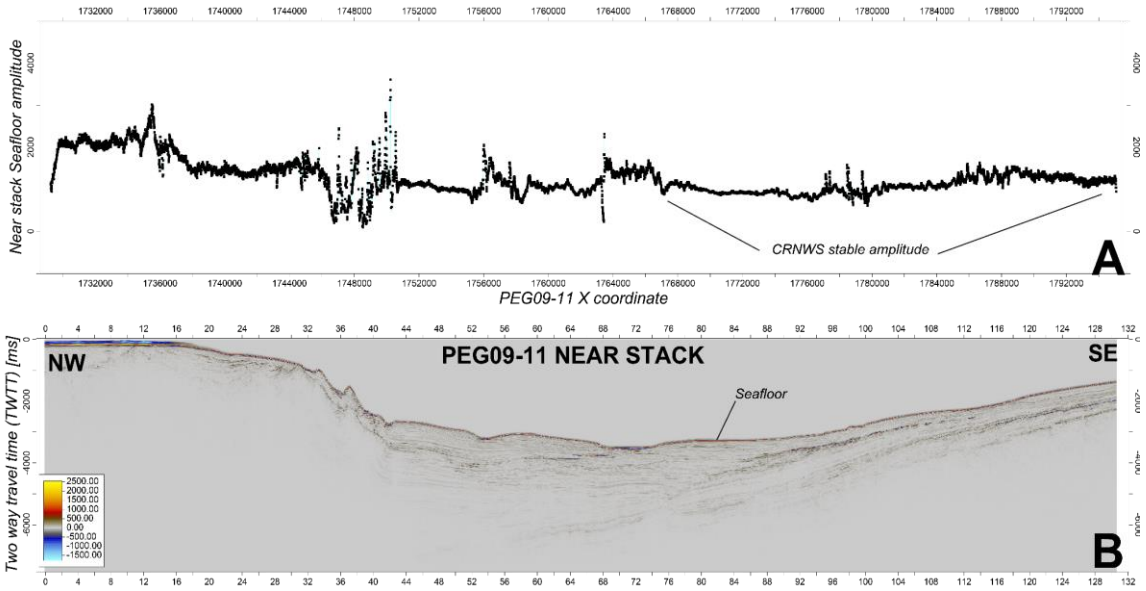

Figure S2. *(A) Plot showing extracted PEG09-11 near-stack seafloor amplitudes plotted against X coordinates. The seafloor X coordinates (meters) displayed on the X axis. Seafloor amplitudes appear stable across the line increasing only in the Hikurangi Channel. (B) PEG09-11 Near-angle stack for reference.*

Text S2.

We present all extracted seismic wavelets used during simultaneous AVO inversion (Figure S3).

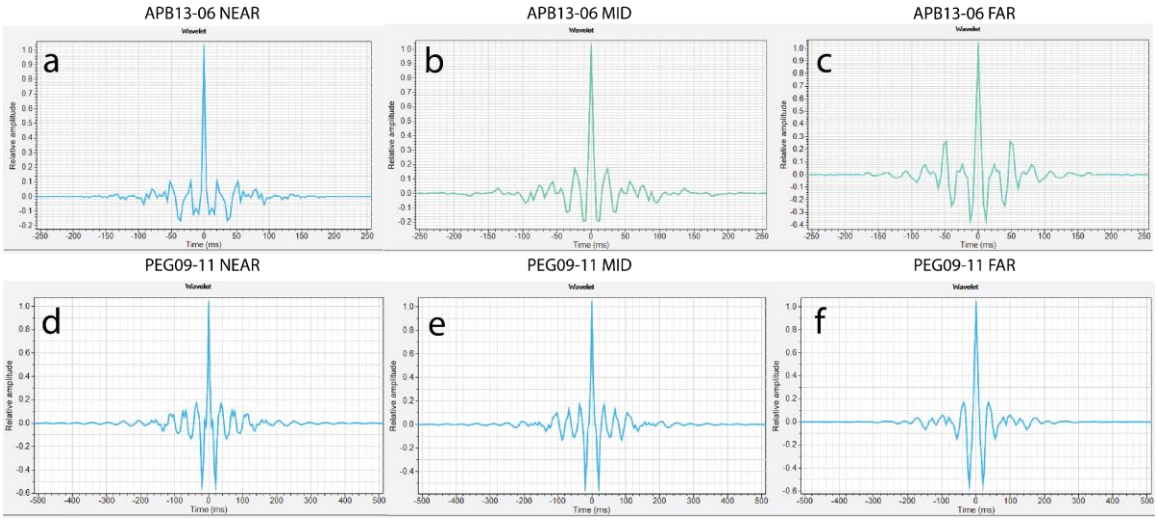

Figure S3. *Six wavelets used for APB13-06 and PEG09-11 simultaneous AVO inversion.*

Text S3.

We present more detailed descriptions of seismic horizons interpreted in our study.

Top HIP

The deepest horizon interpreted in this study is shown in Figure 1 and highlighted in Figure S4 as a yellow-coloured interpretation and labelled 'Top HIP'. The horizon naming convention follows Davy et al. (2008). We interpreted the Top HIP horizon to have the following seismic characteristics:

- Continuous to discontinuous lateral continuity. Sections of this horizon may be laterally continuous from between 500 m to several kilometers. Breaks in the horizons continuity may be marked by sub-vertical interpreted faults or wide-spanning (up to several kilometers) gaps in horizon reflectivity (Figure S4).

- Overlying seismic reflection facies are typically chaotic and low amplitude. Underlying Top HIP, the seismic facies are typically parallel and of similar amplitude to Top HIP for several reflection cycles. The Top HIP horizon appears to mark a downward increase is seismic reflection continuity, with underlying seismic facies being increasing laterally continuous compared with reflections overlying Top HIP (Figure S4).

- A positive reflection polarity. In both surveys, the Top HIP horizon is marked by a red seismic reflection, indicating an increase in reflection coefficient.

• A moderate seismic amplitude. Top HIP is interpreted partially due to the sudden increase in seismic amplitude that it marks at long two way travel times (~7200 ms–9200 ms) (Figure S4). Overlying Top HIP, seismic facies are of typically very low amplitude, appearing almost reflectionless in some areas (Figure S4).

Stratigraphically, Top HIP marks the vertical termination of an (oceanic) large igneous province (O-LIP), previously described through geochemical and seismic analysis as the Hikurangi Plateau (Mortimer and Parkinson, 1996; Davy et al., 2008).

Top Gondwanan Wedge

The second deepest horizon interpreted in the Pegasus Basin AOI is a green horizon labeled 'Top Gondwanan Wedge' (Figure S5). Top Gondwanan Wedge tracks a discontinuity, representing a distinct seismic facies change from ~3000 ms–~8200 ms TWTT (Figure S5 A).

We summarise interpretation criteria for the Top Gondwanan Wedge:

• The overlying seismic facies is interpreted as having: moderately to highly continuous reflections, variable amplitude (although typically moderate to high amplitude), varied reflection frequency.

• Underlying Top Gondwanan Wedge, the seismic facies can be broadly described as having: low reflection continuity and a chaotic reflection character, moderate to low seismic amplitude (amplitudes lower than overlying facies) and varied to high reflection frequency. Despite a highly chaotic internal character, groupings of parallel reflections appearing either horizontal or dipping toward the SE are interpreted within the lower seismic facies.

• Overlying facies onlap the interpreted discontinuity (Top Gondwanan Wedge) under the Hikurangi Trough (Figure S5 B). Southeastward toward the Chatham Rise, overlying facies drape the discontinuity. When Top Gondwanan Wedge reaches ~7000 ms TWTT under the Hikurangi Trough, we interpret increasing similarity between seismic facies bounding the horizon. The typically chaotic underlying facies increases in lateral continuity and seismic amplitudes between facies appear more uniform (Figure S5 B).

Interpretation of the Top Gondwanan Wedge horizon results in the identification of a prominent seismic unit labelled 'Paleo Gondwanan Wedge' (Figure S5 A). We name this seismic unit / stratal interval after previous studies, which interpret the same unit (e.g., Davy et al., 2008; Plaza-Faverola et al., 2012).

Base Sequence Y

Shown in Figure 1 and Figure S6, we interpreted a horizon named 'Base Sequence Y'. The horizon coloured in dark blue tracks a widely observed reflection, seen in most NW-SE trending APB13 and PEG09 lines. We summarise the reflection characteristics of Sequence Y Base horizon that drove interpretation across the AOI:

- The seismic reflection typically has high lateral continuity. We rarely interpret the horizon to be intersected by seismic-scale faults. Within the AOI, fault intersection of Base Sequence Y is typically localized to the Chatham Rise region at depths of ~<4500 ms TWTT.
- The horizon has a negative reflection polarity (blue-coloured reflection in APB13).
- Seismic amplitude of Sequence Y Base is a distinctive feature of the horizon. Across the AOI, Sequence Y Base features an anomalously high seismic amplitude for a reflection at that depth. The base of Sequence Y can often be identified by observation of amplitude alone in the AOI. The reflection's amplitude may be equal to or greater than the seafloor amplitude at the same CDP location (with reversed polarity compared with the seafloor reflection). Although Base Sequence Y is interpreted in some areas with low seismic amplitude, these sections typically punctuate the horizon rather than define it on a seismic line-scale.

We interpret the Base Sequence Y horizon to represent the top of the MES seismic unit which is bound at the base by the Top Gondwanan Wedge horizon (Figure S5). The name of MES follows Davy et al. (2008)'s naming convention for a several hundred meter to ~2 kilometer thick Mesozoic sedimentary sequence that overlies the paleo Gondwanan accretionary wedge. It was identified in Davy et al. (2008) as a transparent to weakly reflective, laminar interval with an interval velocity of 2300-2500 m/s.

Top Sequence Y

Shown in Figure 1 and Figure S7, we interpreted a horizon named 'Top Sequence Y'. The horizon coloured in red tracks a widely observed reflection, seen in most NW-SE trending APB13 and PEG-09 lines. Top Sequence Y is also interpreted in SW-NE trending lines, allowing loop-tie interpretation to be done within the AOI. Defining reflection characteristics of Top Sequence Y are summarised:

- The seismic reflection has high lateral continuity. We rarely interpret the horizon to be intersected by seismic-scale faults. Within the AOI, fault intersection of Top Sequence Y is typically localized to the Chatham Rise region at depths of ~<4500 ms TWTT.
- Top Sequence Y has a strong, positive reflection polarity (red-coloured reflection in APB13).
- Seismic amplitude of Top Sequence Y is a distinctive feature of the horizon. Across the AOI, Sequence Y Top features an anomalously high seismic amplitude for a reflection at that depth. The reflection's amplitude may be equal to or greater than the seafloor amplitude at the same CDP location (with the same polarity as the seafloor reflection). Although Top Sequence Y is interpreted in some areas with low seismic amplitude, these sections typically punctuate the horizon rather than define it on a seismic line-scale.

The top Sequence Y horizon interpreted in this study correlates to the horizon 'Reflector 7', interpreted within Barnes et al. (2010) and Plaza-Faverola et al. (2012). Interpretation of Sequence Y Top results in the formation of a third seismic unit labelled "Sequence Y" (Figure S6 B, C). We interpret Sequence Y to overlie MES across the AOI as a generally thin unit that thickens to the SW on the Chatham Rise. We name the unit Sequence Y after previous interpretations by Wood and Davy (1994); Davy et al. (2008); Plaza-Faverola et al. (2012) and Crutchley et al. (2020). Sequence Y is a 100-200 ms thick, widely interpreted interval across the Hikurangi Trough, Chatham Rise and Hikurangi Plateau (Davy et al., 2008). The unit is described by previous authors as being a prominent high amplitude, continuous reflection sequence that contains several unconformities (Carter et al., 1999). Sequence Y is regionally significant, being identified as a condensed sequence of mudstone and chalk that deposited from ~70 Ma–~30 ma. On the Chatham Rise as ODP site 1124, Sequence Y was sampled as a sequence of nannofossil chalks alternating with

mudstones (Carter et al., 1999). In addition to several unconformities identified within Sequence Y, the Marshall Paraconformity (27–33 Ma) was interpreted to bound the upper surface of Sequence Y (Carter et al., 1999). Recognized as a regional Oligocene-aged feature of New Zealand, the Marshall Paraconformity formed through widespread erosion of the seafloor ~23 Ma and has been linked to the onset of the Deep Western Boundary Current's (DWBC) influence in the southwest Pacific (Carter and McCave, 1994).

In seismic stratigraphic studies of the northwestern Chatham Rise by Barnes (1994) and Barnes (1994a), a "very strong reflection" labelled 'Reflector O' was identified within single channel seismic data. Through stratigraphic correlation to distal exploration wells, Reflector O was interpreted to mark the top of an Oligocene-aged Sequence later known as Sequence Y (Wood et al., 1989; Carter et al., 1999).

Horizon L

The youngest interpreted horizon in the AOI is shown as a light, blue-coloured horizon in Figure 1 and Figure S8. Horizon L tracks a widely observed reflection termination boundary, interpreted as an unconformity on the Chatham Rise that deepens northwestward under the Hikurangi Trough (Figure S7 A). Shown in Figure S8, Horizon L deepens before terminating against the Top Sequence Y horizon. Identification of Horizon L is made through interpretation of clear onlap of reflections onto Horizon L (Figure S8). We interpret Horizon L over much of the AOI, shoaling on the Chatham Rise and terminating under the central Hikurangi Trough (Figure S8). In Figure S8, the black dotted line shows the point where Horizon L downlaps onto the Top Sequence Y horizon.

To the west of the AOI, Horizon L extends across the Hikurangi Trough, approaching the modern deformation front, however to the east, the unconformity is distal from the deformation front, consistent with increasingly broad overlying Hikurangi Trough sequence (Figure S8). The interpretation of Horizon L forms the upper boundary of a wedge-shaped seismic unit positioned between the Top Sequence Y horizon and Horizon L (Figure S8 A). Generally, this interval of Chatham Rise cover material is consistently interpreted as low amplitude, highly continuous facies that are increasingly faulted to the south of the AOI.

Horizon L is a regional unconformity located on the Chatham Rise slope and previously identified by Barnes (1994) and Plaza-Faverola et al. (2012). Horizon L is described in the northwestern Chatham Rise as being "a very prominent onlap surface (labelled L), that is truncated by erosion on the rise crest, can be traced widely beneath the slope". Dating of Horizon L came from three Pleistocene-Pliocene cores in the region. Chronostratigraphally Horizon L approximately delineates two New Zealand age stages ~3.6 Ma, the Waipipian and Opoitian (Barnes, 1994a). Horizon L is the oldest in a series of Mid Pliocene (~3.6 Ma) to Late Pleistocene (~0.1 Ma) erosive unconformities thought to be associated with strong bottom current activity on the northwestern Chatham Rise, which formed both erosive scours and depositional drift features (Barnes, 1994). Horizon L is thought to have formed from a period of intense Mid Pliocene erosion, induced by current action on the Northwestern Chatham Rise (Barnes, 1994). It is speculated that unconformity L is possibly coincident with a global climatic cooling event (~3.2 Ma), characterized by potentially increased Antarctic glaciation (e.g., Kennett and Von der Borch, 1986) and bottom water cooling (Joyce et al., 1990; Barnes, 1994).

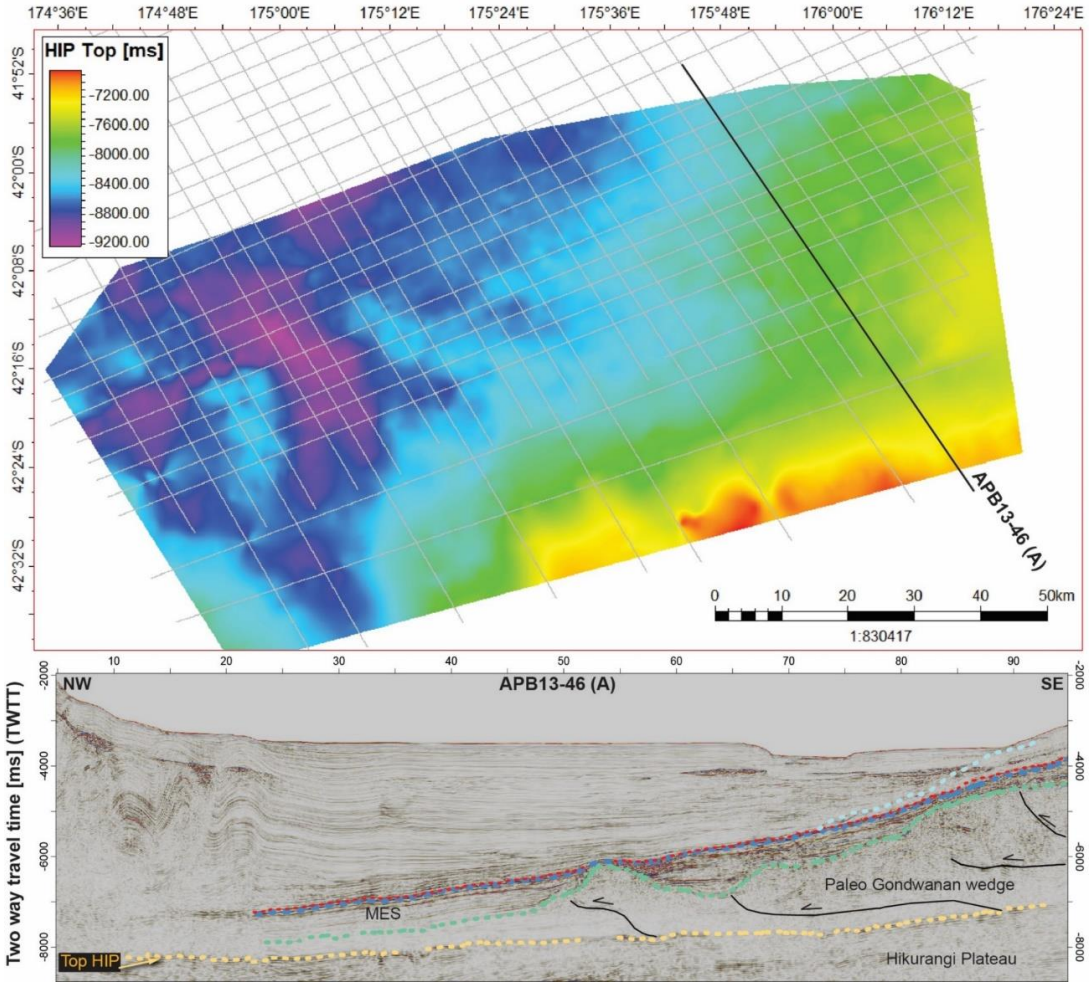

Figure S4. *(Top) Structural map in time (TWTT) showing the interpreted top HIP horizon. The yellow-coloured HIP top horizon tracks a continuous to discontinuous, positive polarity reflection that marks an increase in seismic amplitude at TWTTs from ~7200–~9200 ms TWTT. The structural map shows the Top HIP surface to generally deepen toward the W to SW, and shoal under the eastern Chatham Rise. (A) APB13-46 showing the Top HIP horizon deepening to the NW under the Hikurangi thrust belt. Multiple large thrust faults (black lines)*

are interpreted to splay from the Top HIP horizon and imbricate the Paleo Gondwanan Wedge.

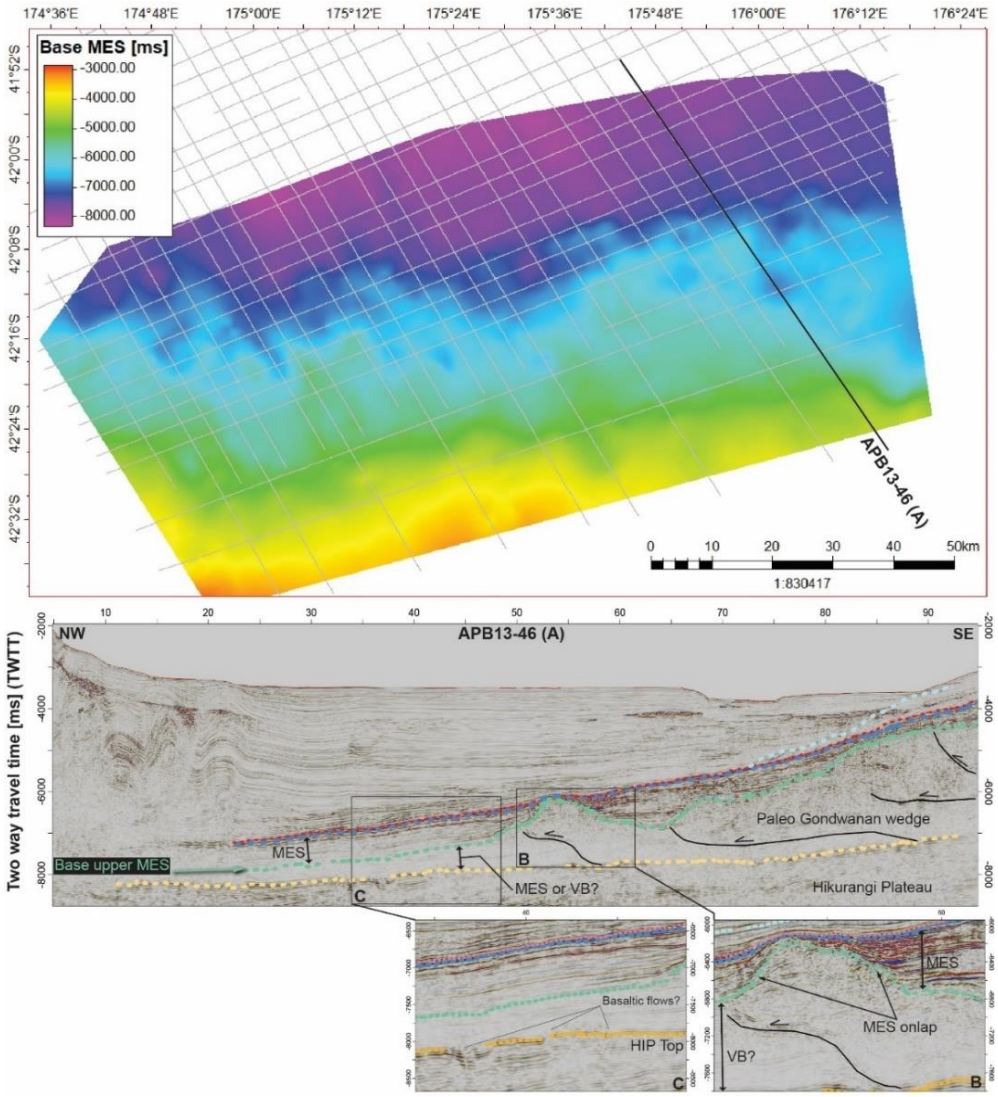

Figure S5. *(Top) Structural map in time (TWTT) showing the interpreted surface named 'Top Gondwanan Wedge'. In the study area, Base upper MES is shallowest under the Chatham Rise to the SW and deepens to the north. (A) Seismic line APB13-46 highlighting Top Gondwanan Wedge in green. (B) Zoomed window showing clear onlap of MES reflections terminating against Paleo Gondwanan Wedge reflections and a large, interpreted frontal thrust. (C) Zoomed window highlighting HIP Top surface and interpreted Top Gondwanan Wedge horizon. Ambiguity of the Top Gondwanan wedge NW of the thrusted Gondwanan*

Wedge material is clear. VB, Volcaniclastic basement. MES, Mesozoic sedimentary sequence.

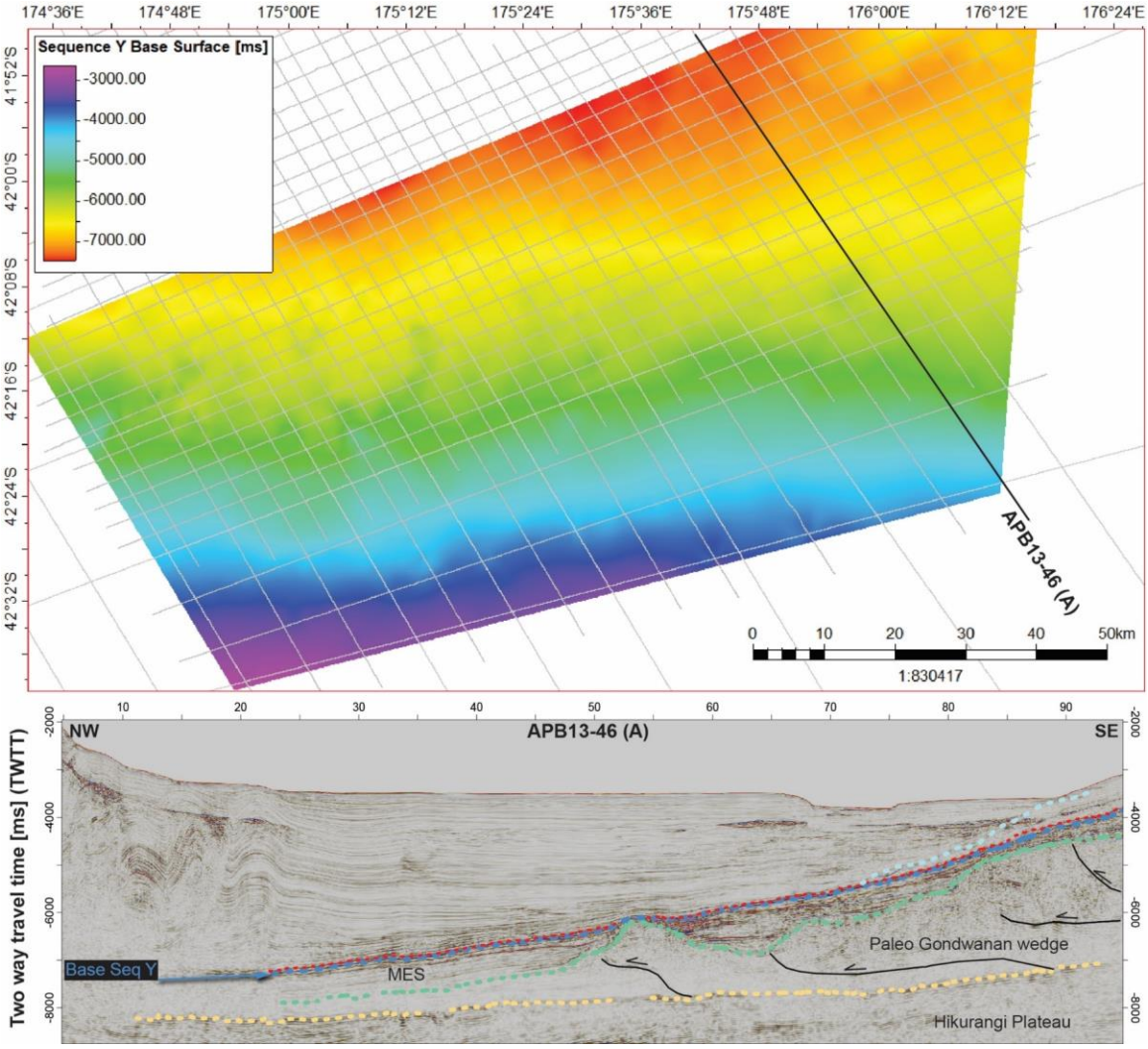

Figure S6. *(Top) Structural map in time (TWTT) showing the interpreted Sequence Y Base horizon. In general, the horizon is deepest to the north reaching depths of >7000 ms TWTT. The horizon is shallowest to the SW on the Chatham Rise.*

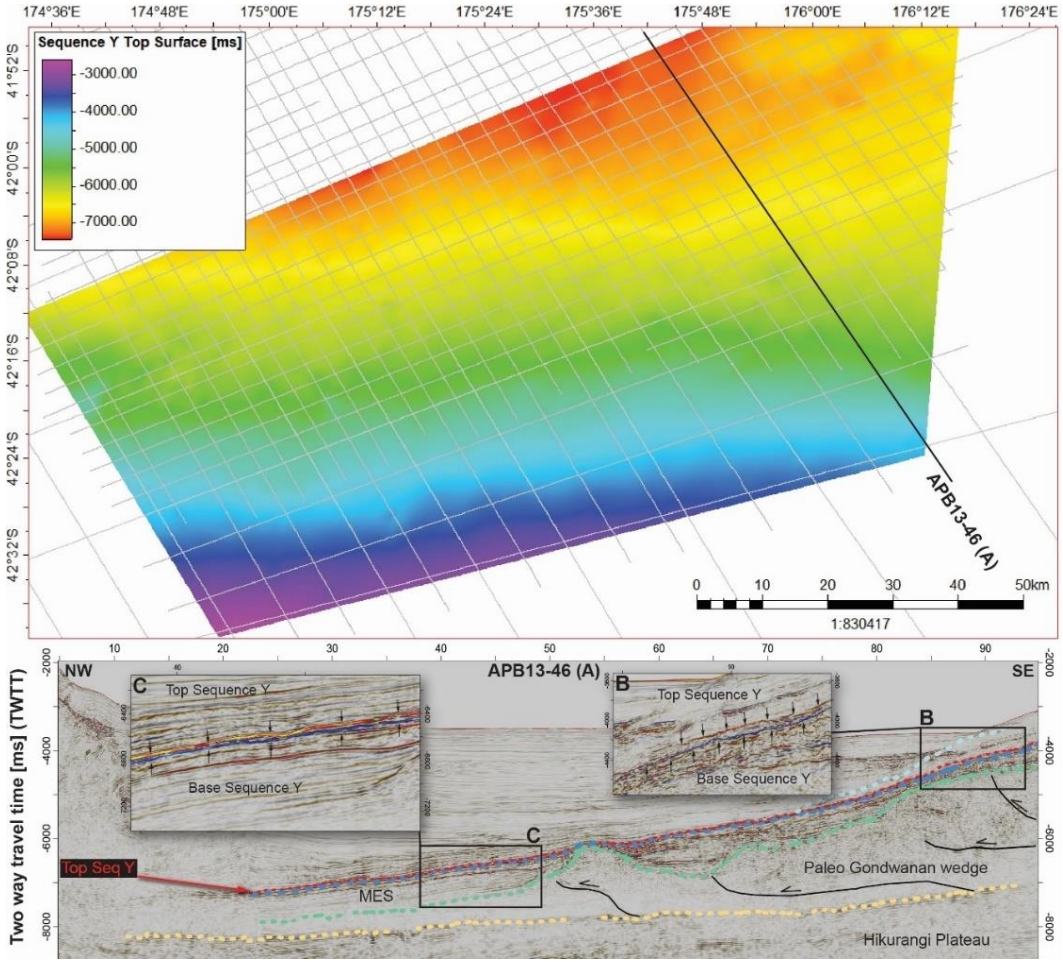

Figure S7. *(Top) Structural map in time (TWTT) showing the interpreted top of Sequence Y. Similarly with the Base of Sequence Y, the horizon is deepest to the north reaching depths of >7000 ms TWTT. The horizon is shallowest to the SW on the Chatham Rise. (A) Seismic line APB13-46 highlighting the Top Sequence Y horizon, showing the concordance between Sequence Y base and Sequence Y top. The Mesozoic sedimentary sequence (MES) interval is*

interpreted to abut and pinch-out against a mounded area of Paleo Gondwanan Wedge material to the center of the line.

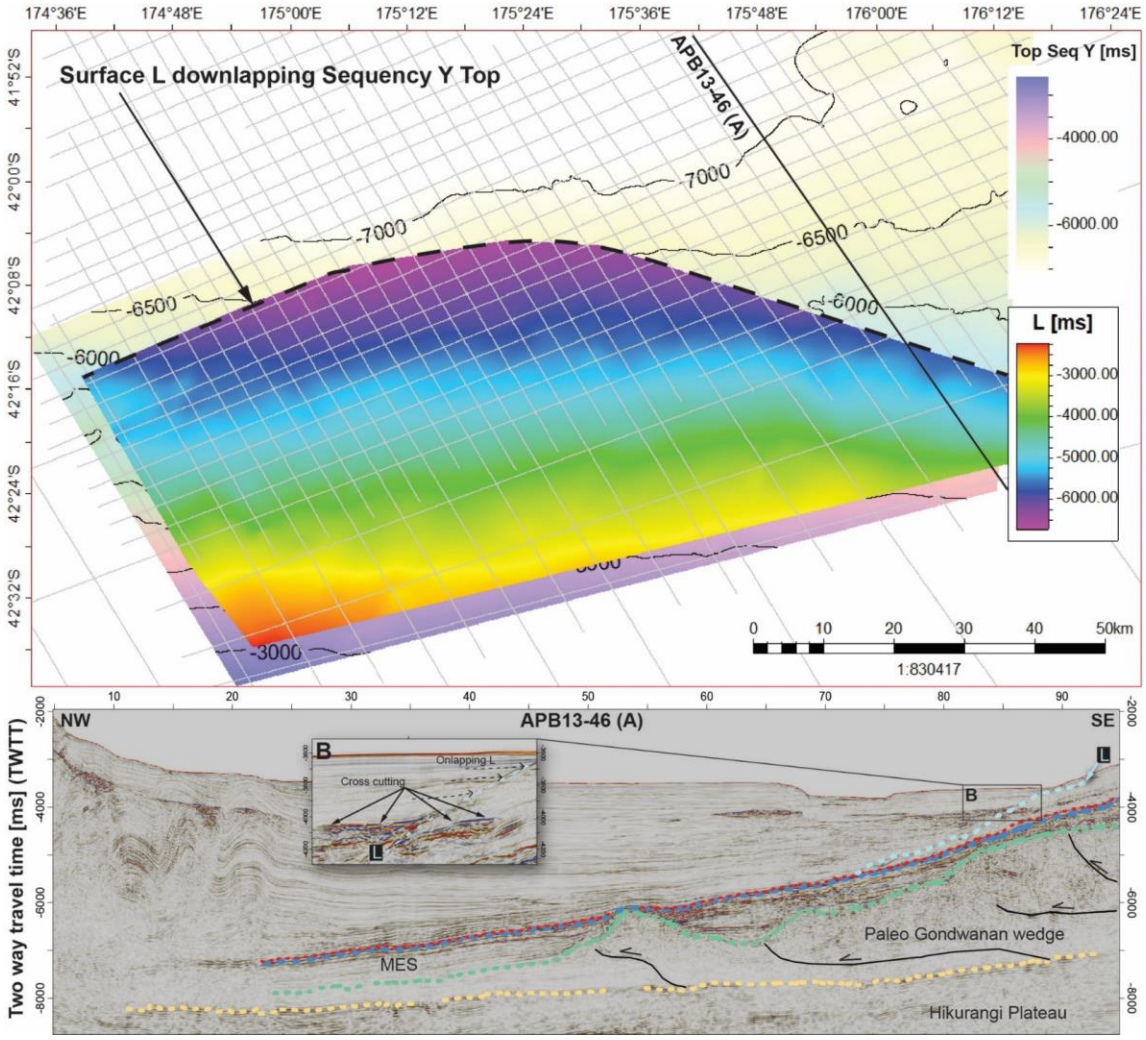

Figure S8. *(Top) Structural map in time (TWTT) showing the interpreted extent of the regional unconformity L. Horizon L shallows to the southwest of the Chatham Rise, deepening northward. The black dotted line shows the point of Horizon L downlap onto Sequence Y Top. The pastel coloured structural map underlying L is the Sequence Y Top horizon depth (TWTT). (A) APB13-46 highlighting horizon L. (B) zoomed section showing*

overlying onlap onto L and cross-cutting, high amplitude reflections within the Top Sequence Y – L interval.

Text S4.

Sequence Y reflectivity

Extracted RMS amplitude data from near and far angle stacks are shown in Figure S9. We highlight four regions where amplitude changes with angle are clear. Location 2 on the CRNWS in Figure S9 is the focus in this study. Top Sequence Y horizon forms the upper bound to the Sequence Y unit interpreted in this study (Figure 1). In pre-stack processed near angle data, the Top Sequence Y horizon shows generally consistent RMS amplitude across the study area (Figure S10) To the southwest on the CRNWS, we observe broadly higher amplitudes than the central study area. In near stack data, the Top Sequence Y horizon is most reflective to the far east of the study area under the Hikurangi Trough (Figure S10 Location A). Up dip from Location A (Figure S10), Top Sequence Y's RMS amplitude increases onto the shoaling Chatham Rise. In far angle pre-processed stacks, we highlight two areas (C, D) where RMS amplitudes are observed to vary the most between angle stacks (Figure S10).

MES reflectivity

Directly underlying Sequence Y, we investigate the interpreted MES unit bound between the base of Sequence Y and top of the Gondwanan Wedge (Figure S11 B). Using full angle stacks, we sample average RMS amplitude values across the thickness of MES (Figure S11 A). RMS amplitudes within the MES are observed as weakest with depth, toward the north (Figure S11 A). As MES shoals southward, a unit-wide increase in RMS amplitude is observed across the study area (Figure S11 A). Two localities of anomalously high amplitude are observed to the east and west of the study area, appearing as red-coloured zones (Figure S11 A). Further southward, MES decreases in RMS amplitude onto the Chatham Rise. In Near angle data, the RMS amplitude of the MES interval is observed to strengthen from the NW to the SE (Figure S12 A). The highest RMS amplitude values are generally seen to the SE on the Chatham Rise where MES is shallowest (<1500 ms TWTT below the seafloor). In far angle data, the RMS amplitude of MES stays generally similar to

near angle data (Figure S12 B). Despite this, an increase in RMS amplitude values of MES is observed to the east of the study area deep under the Hikurangi Trough (Figure S12 A, B). Within the MES interval, we do not interpret noticeable AVO effects on the Chatham Rise comparable to Sequence Y reflections (e.g., Figure S9; Figure S10). Full angle data does highlight regions of high amplitude MES, however angle stack data does not indicate these regions to change significantly in amplitude with angle.

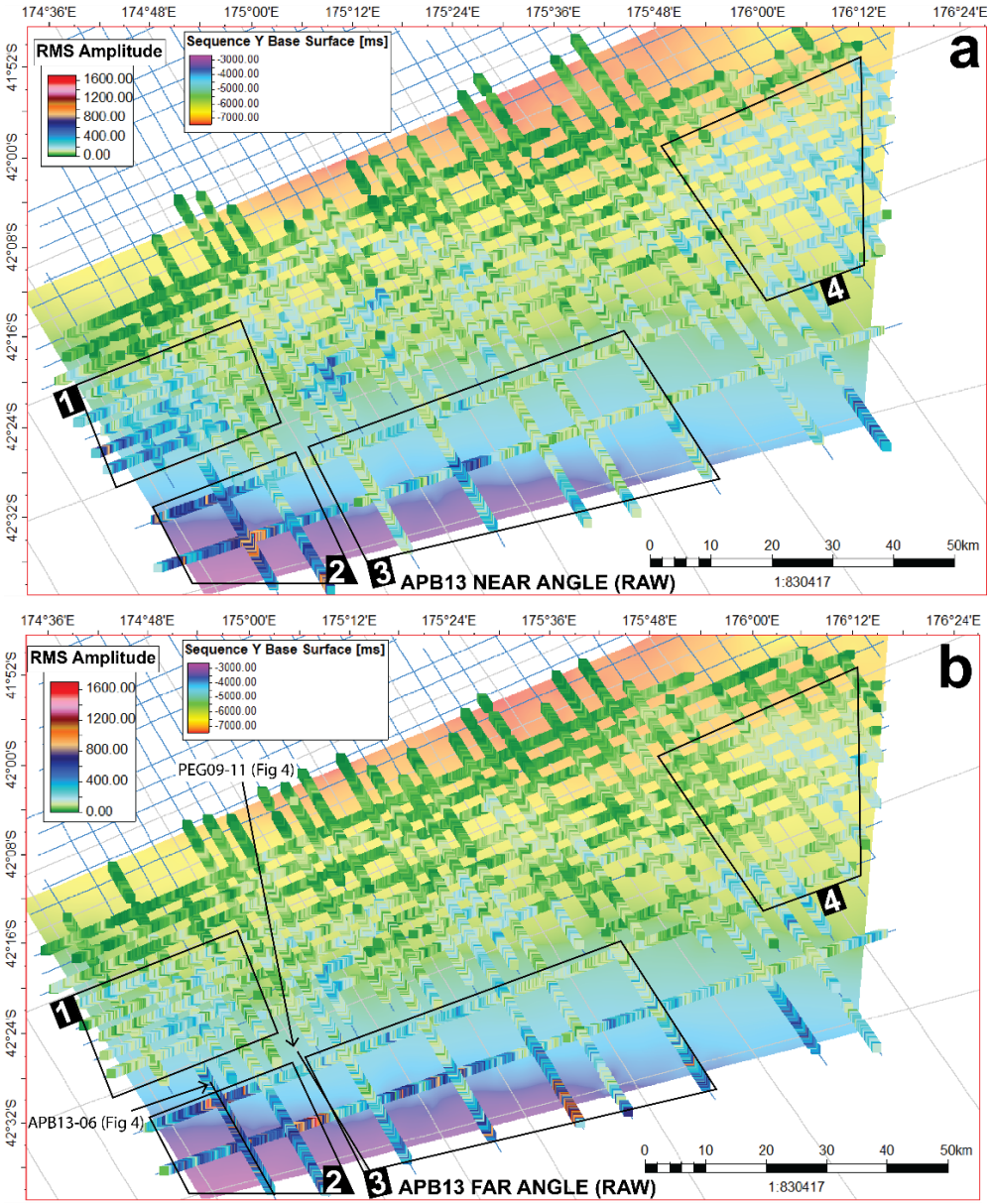

Figure S9. *(a) Map showing Base Sequence Y structural map. Overlain is the Base Sequence Y root mean square (RMS) amplitude extracted from near angle APB13 data (pre-stack*

processing). (b) Far angle Base Sequence Y RMS amplitude overlying Base Sequence Y structural map. Four regions are highlighted by black boxes in each map, due to clear changes in amplitude with increasing angle.

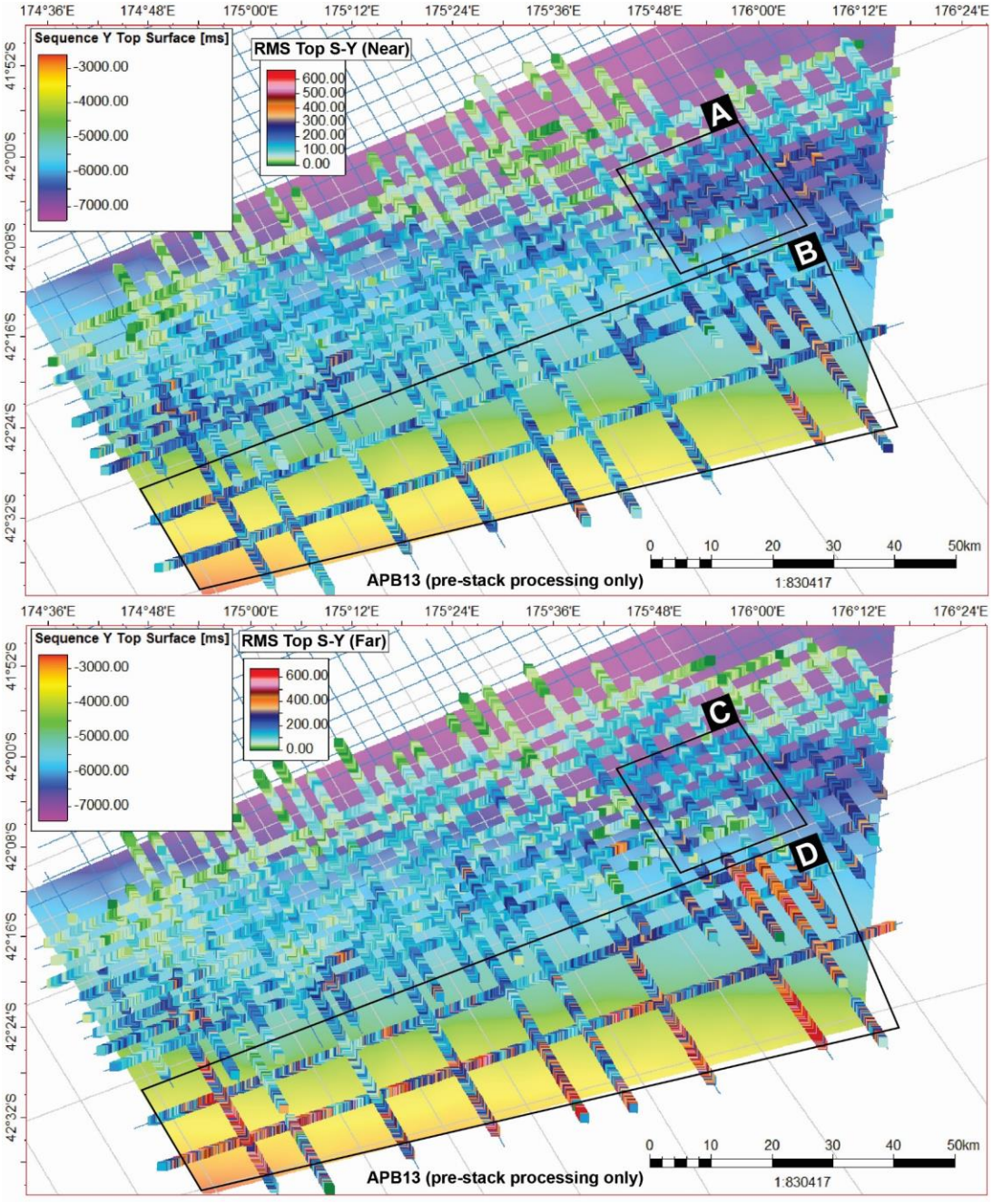

Figure S10. *(Top) Top Sequence Y (S-Y) structural map in time overlain with near stack root mean square (RMS) amplitudes extracted from the Top Sequence Y horizon (APB13 pre stack processing). Two locations of notable amplitude change with angle are highlighted (A-B).*

(Bottom) Top Sequence Y (S-Y) structural map in time overlain with far stack RMS amplitudes extracted from the Top Sequence Y horizon. Two locations of notable amplitude change with angle are highlighted (C-D).

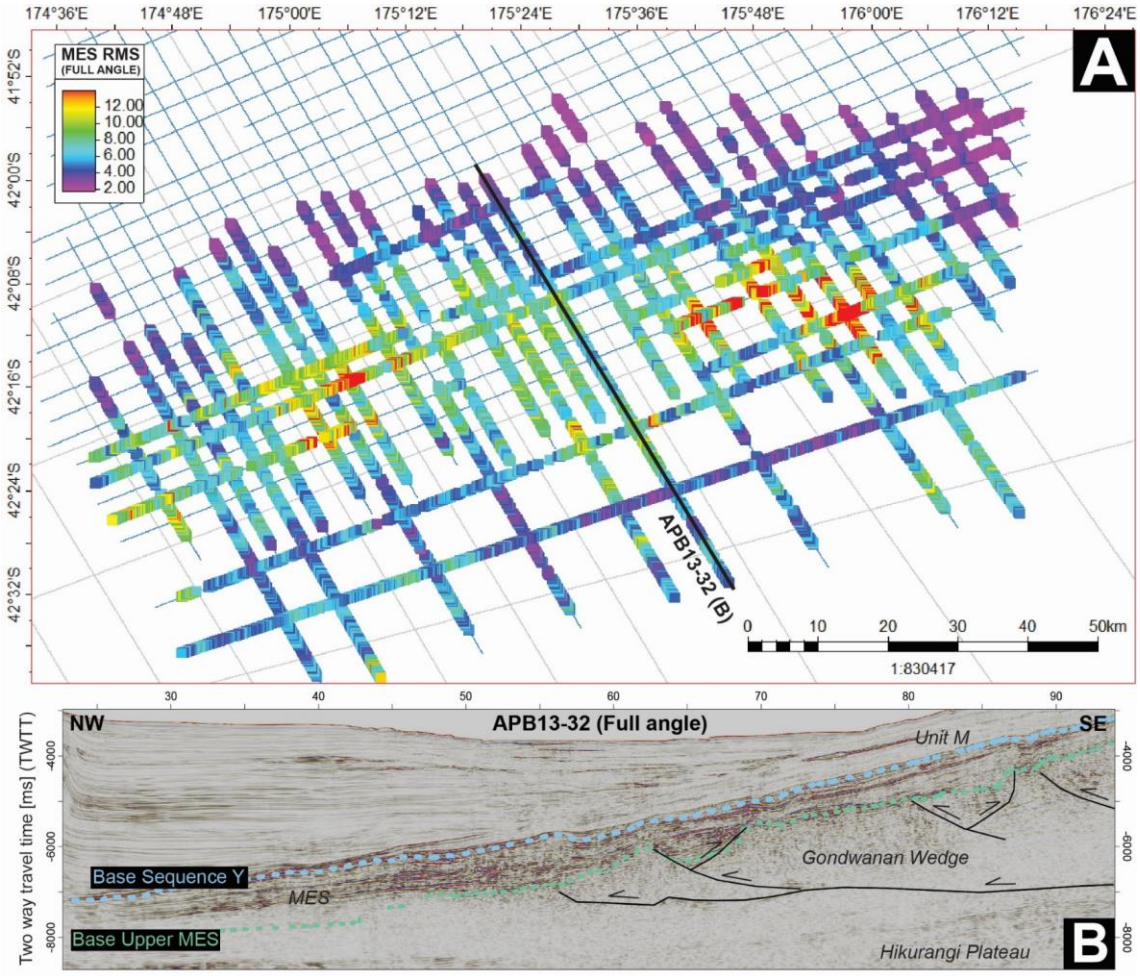

Figure S11. *(A) Root mean square (RMS) amplitude map the Mesozoic sedimentary sequence (MES) unit. RMS amplitude calculated along each line between the Base Upper MES horizon and the Base Sequence Y horizon. Warming = stronger amplitudes A trend in the AOI of increasing RMS amplitude to the SE is interpreted beginning approximately SE of the deformation front. MES RMS amplitude increases to the SE before decreasing under the Chatham Rise. APB13-32 line location marked. (B) APB13-32 (Full angle) seismic line showing the MES unit, which RMS amplitude was measured from. The MES unit thickness is*

generally consistent in this area of the AOI with no Gondwanan Wedge thrusts interrupting the unit.

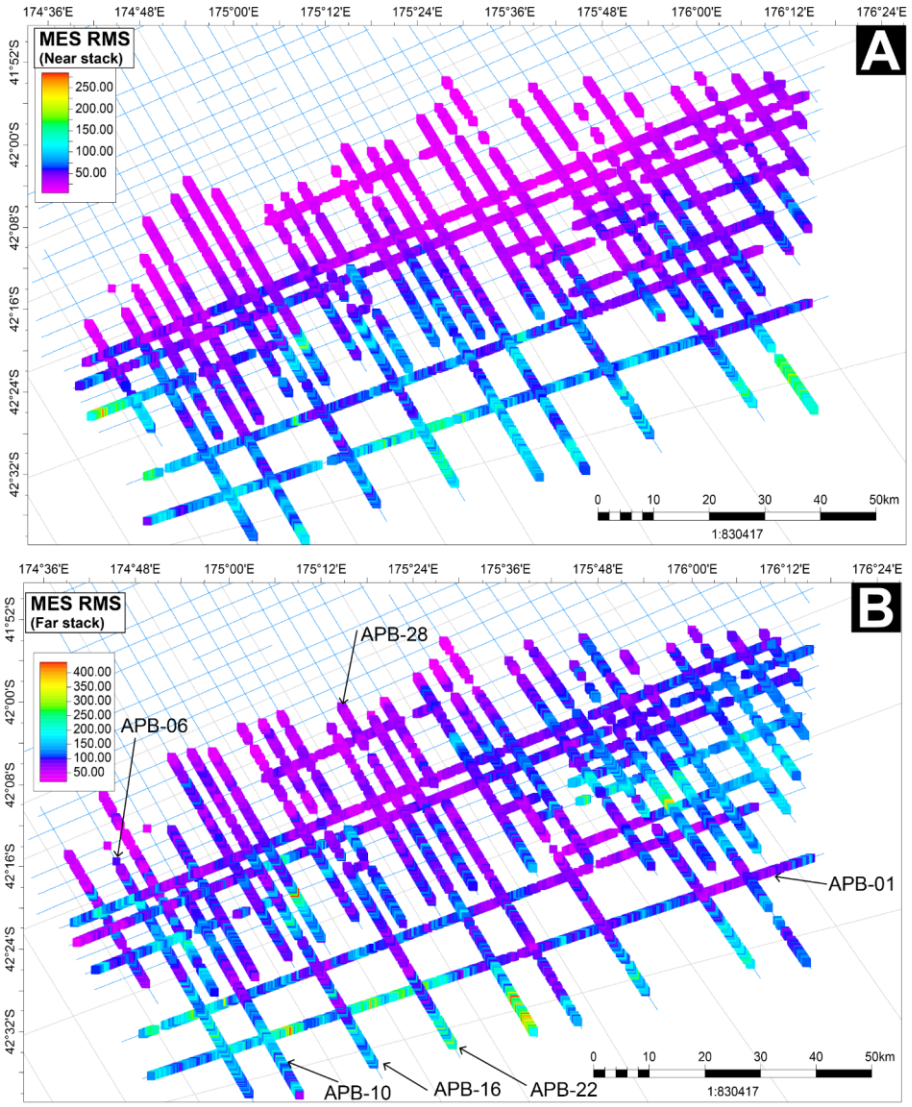

Figure S12. *(A) Root mean square (RMS) amplitude attribute using near angle data for the Mesozoic sedimentary sequence (MES). Warming = stronger amplitudes. (B) RMS amplitude attribute data for far angle data. Labelled APB lines are focused on during following analysis.*

Text S5.

We present Figure S14, which highlights distinct clustering of background trend points compared with BSR and Sequence Y samples (sampled from Figure S13).

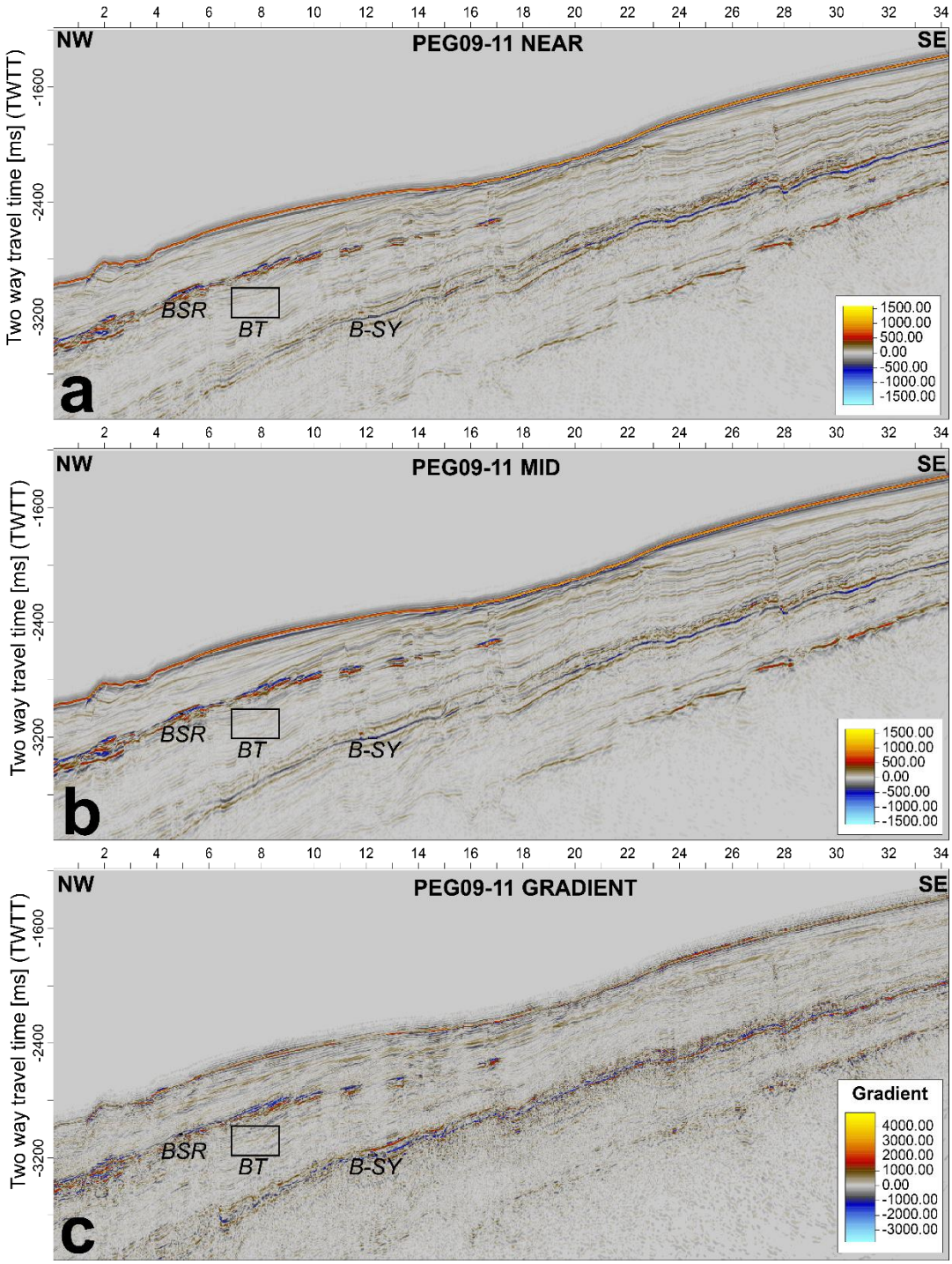

Figure S13. *Three seismic stacks used for crossplotting stacks against the gradient. VOIs are overlain. BT, Background Trend VOI. B-SY, Base Sequence Y VOI sampling the Base Sequence Y negative polarity reflection. BSR, VOI that sample the negative polarity Bottom Simulating Reflection. VOIs are used for crossplotting and identification of multiple data clusters in*

Figure E2. (a) PEG09-11 near angle stack. (b) PEG09-11 mid angle stack. (c) PEG09-11 gradient stack.

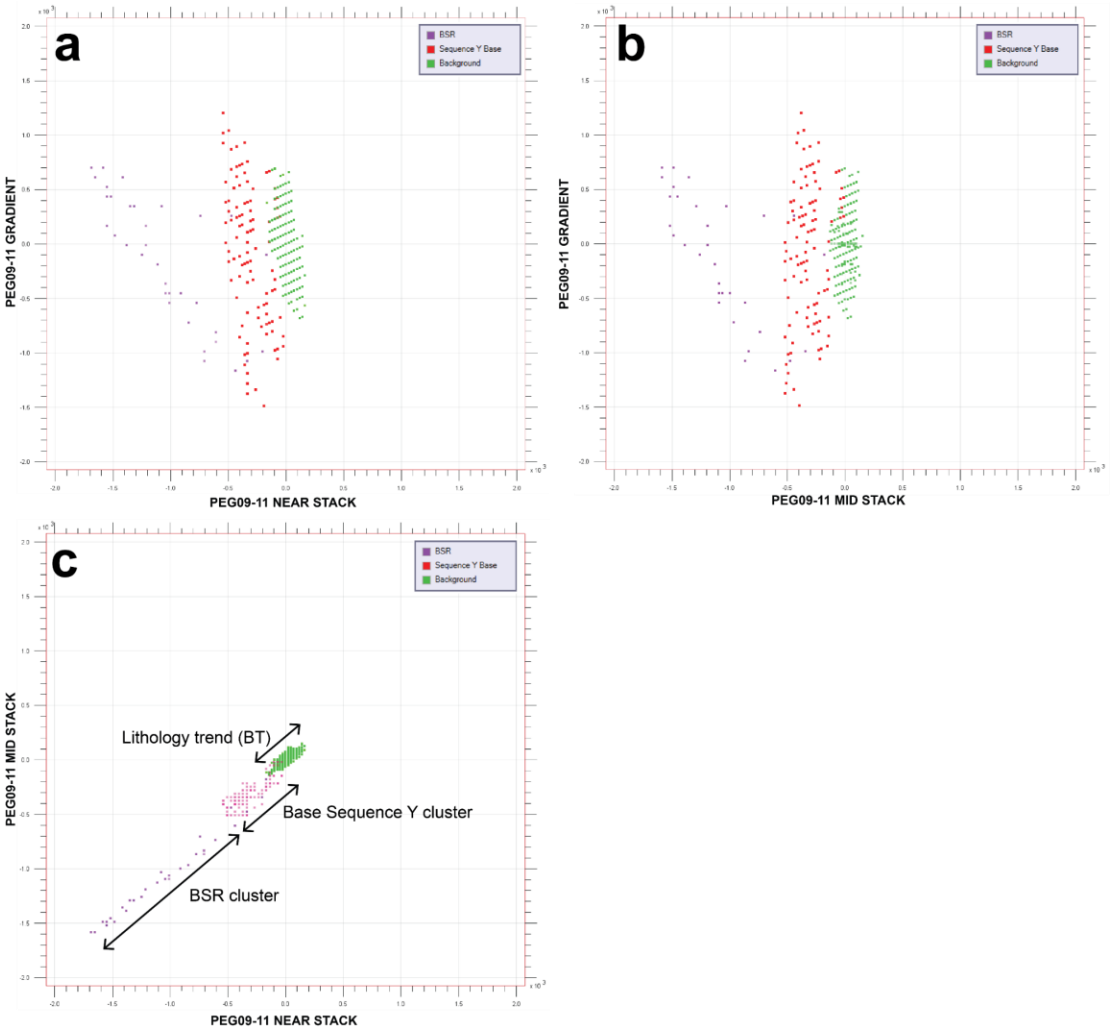

Figure S14. *All crossplot sample locations (VOI) are shown in Figure E1. (a) Crossplot of the Near Stack against the Gradient. Three VOI samples are crossplotted. The Background Trend (BT) VOI sample appears as green points. The Sequence Y Base VOI shows data points (red) clustered to the left of the background trend. The BSR VOI represented by purple data points sits clustered further to the left of the Base Sequence Y trend. (b) The mid stack crossplotted against the gradient stack. (c) The near stack amplitudes crossplotted against the mid stack*

amplitudes. Three VOI are crossplotted and show distinct clustering, suggesting a noise-free background trend.

Text S6.

Figure S15 shows how large gradient values (>-3000) in APB13-06 are not characteristic of the Base Sequence Y reflection.

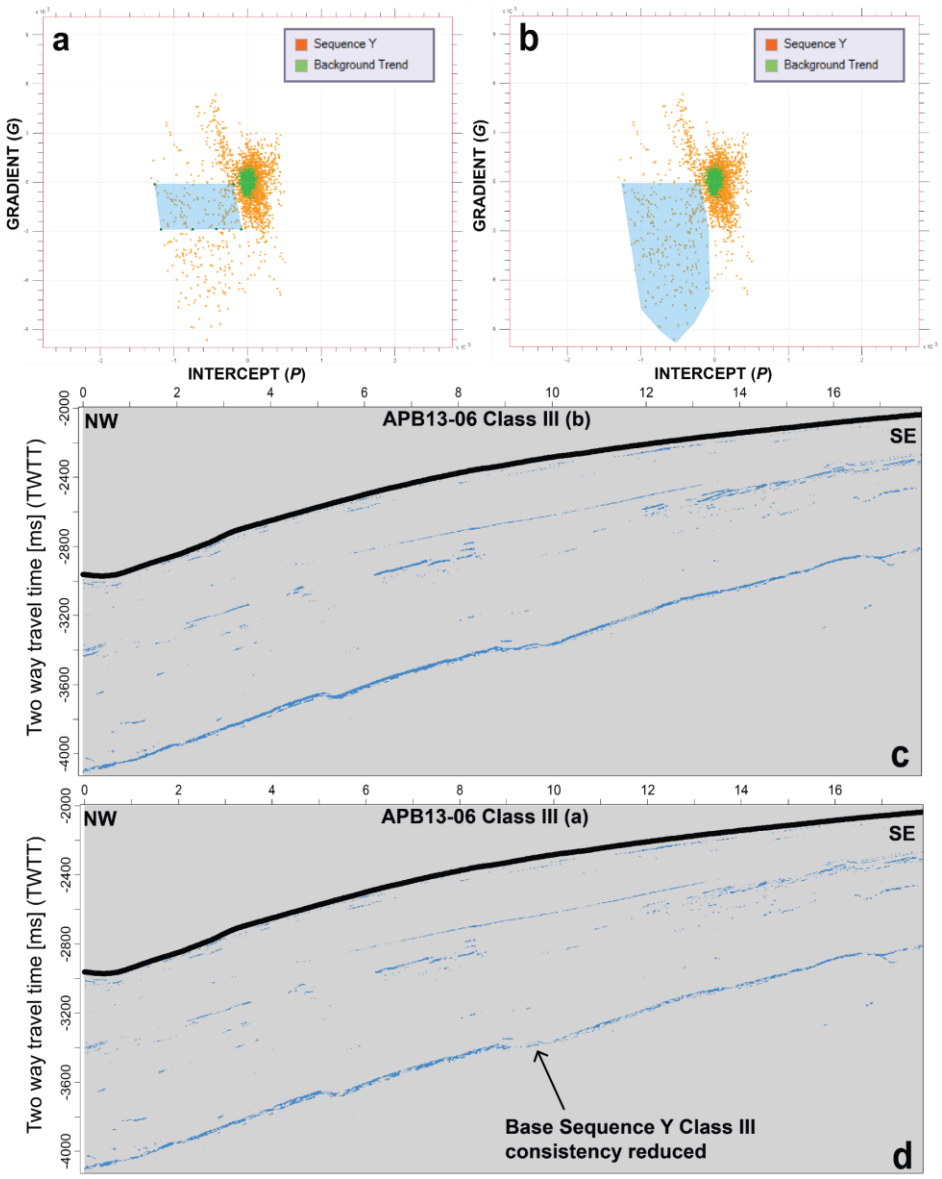

Figure S15. *(a) APB13-06 crossplot with Class III polygon selection omitting large -G values. Values shown in (c). (b) APB13-06 crossplot with larger Class III polygon selection*

encompassing all G values. Values plotted in (d). (c) Points from window B plotted onto seismic. Base Sequence Y and the BSR are well imaged by this Class III AVO anomaly. (d) Class III points from window A plotted onto seismic (omitting larger negative G values).

Table S1.

Table S1 presents Pseudo-3D seismic survey geometry.

Parameter	**PEG09 3D**	**APB13 3D**
Inline number	10	5
Inline step number	1	1
Inline spacing (m)	88.9	120
Crossline number	Varies with individual line	Varies with individual line

Table S1. *Converted 2D-3D survey geometries. All limited angle range stacks (including full angle stacks) were converted to 3D cubes. Note that original survey acquisition parameters outlined in Table 1 did not change.*

Text S7.

We interpret a curved P-impedance vs Vp/Vs trend (Figure S16 a, b) in VOI 3 and VOI 4. In the top left of the cross plots, we observe low P-impedance and high Vp/Vs values associated with the seafloor (Figure S16 a, b). VOI 3 (Figure 10 a) targeted the BSR to the NW. The BSR is interpreted through selecting values that diverge from the trend into lower

P-impedance values (Figure S16 a). The sub-BSR region does not correlate with a reduction in Vp/Vs in this case.

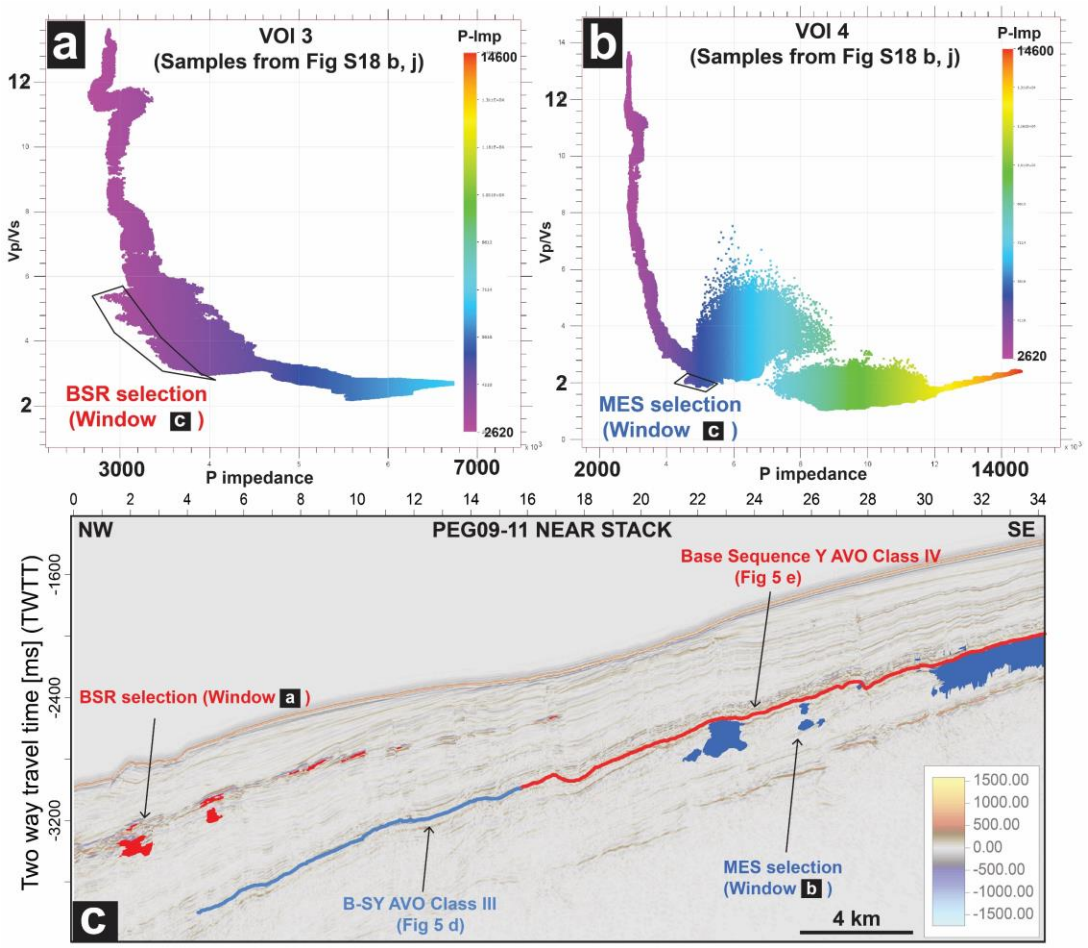

Figure S16. *(a) Vp/Vs cross plotted against P-impedance from VOI 3. Highlighted section (black boxes) shown in window c. (b) Vp/Vs cross plotted against P-impedance from VOI 4. Highlighted section of low P-impedance and Vp/Vs in window c. (c) PEG09-11 near stack with interpretations of amplitude variation with offset (AVO) Classes at Base Sequence Y overlain. Anomalies from windows (a) and (b) are overlain.*

Text S8.

We modeled 'low porosity' marl and sandstone MES with both 100% brine saturation (Appendix Figure S17 a, b). These porosity values are considered low when referring to predicted CRNWS MES porosities by Crutchley et al. (2020). To model a 33% porosity marl

consisting of 50% clay and 50% calcite, we sampled Vp, Vs, ρb and porosity values from ~770 mbsf in U1520C (Unit IV) (IODP, 2018; Wallace et al., 2019). Modelling of this brine-saturated marl resulted in a reflectionless MES unit boundary, owing to near the uniform physical properties of the two layers (Figure S17 a, b).

A 15% gas saturation was substituted using Gassmann equations. In a low porosity marl with gas, we observe an initial decrease in absolute RC at mid angles (~32° AOI) before an inversion of gradient to negative at far angles (~40-45° AOI) (Figure S17 b). This Class III behaviour does not replicate observations in the CRNWS, as mid angle data shows a clear Class III before far angles. To model a sandstone-based MES of 10% clay and 90% quartz with 35% porosity, we calculated an effective media mixture to glean Vp, Vs and ρb (Wang, 2001; Wallace et al., 2019; IODP, 2018).

While Vp/Vs were similar to Unit V MES, Vp of a 35% porosity MES is expectedly higher than ~45% porosity MES. Both low porosity MES lithologies do not represent seismic observations on the CRNWS (e.g., Figure 4). We selected a saturation of 15% to test the impact of the 'gas effect', which is most pronounced at relatively low gas saturations (Figure S17 c, d; Simm, 2007).

In both lithologies, we observe a negative PP RC, 'dimming' slightly to 32° AOI. In the marl, a Class III is interpreted when the far angles (~45°) are gleaned. These outputs do not effectively model Shuey two-term Class III AVO results or broader angle stack amplitude observations (Figure 4). As a mid-stack Class III response was not achievable with these porosities and gas saturations, we explore the effects of increased porosities and gas saturations (Figure 8).

Appendix j: Low porosity MES Zoeppritz modelling

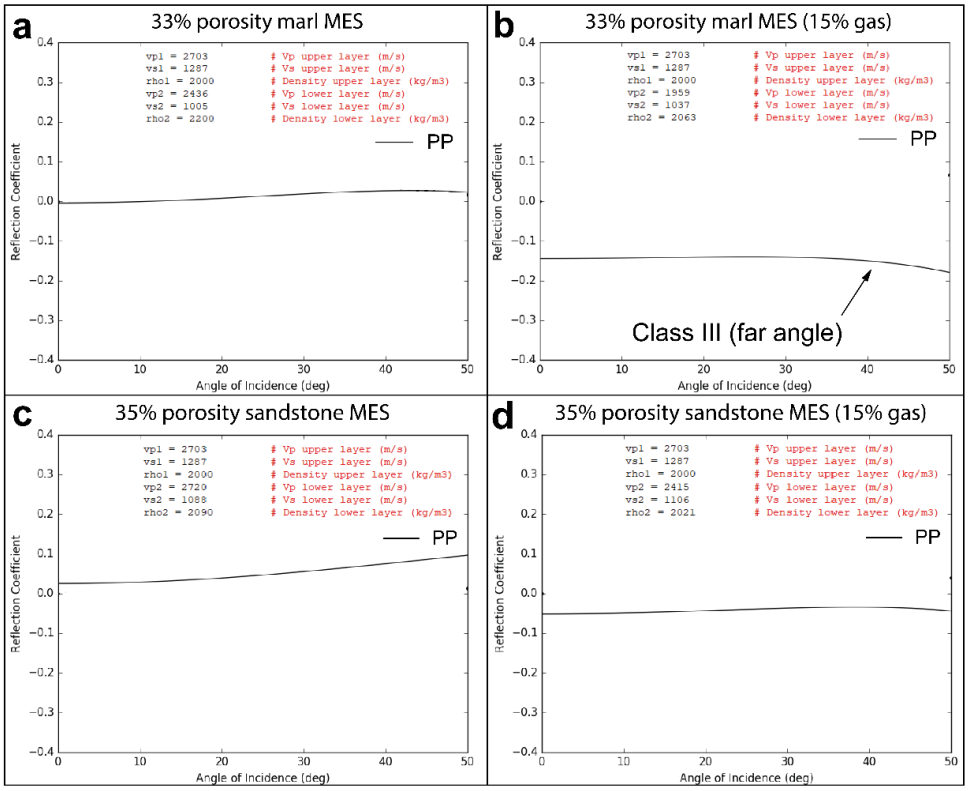

Figure S17. *Low porosity marl Mesozoic sedimentary sequence (MES). (b). Low porosity marl MES with a 15% substituted gas saturation. (c) Low porosity sandstone MES.. (d) Low porosity sandstone MES substituted with 15% gas saturation.*

Text S9.

We show full-length inverted seismic data in Figure S18. Inset black boxes in Figure S18 represent inverted sections shown in Figure 7.

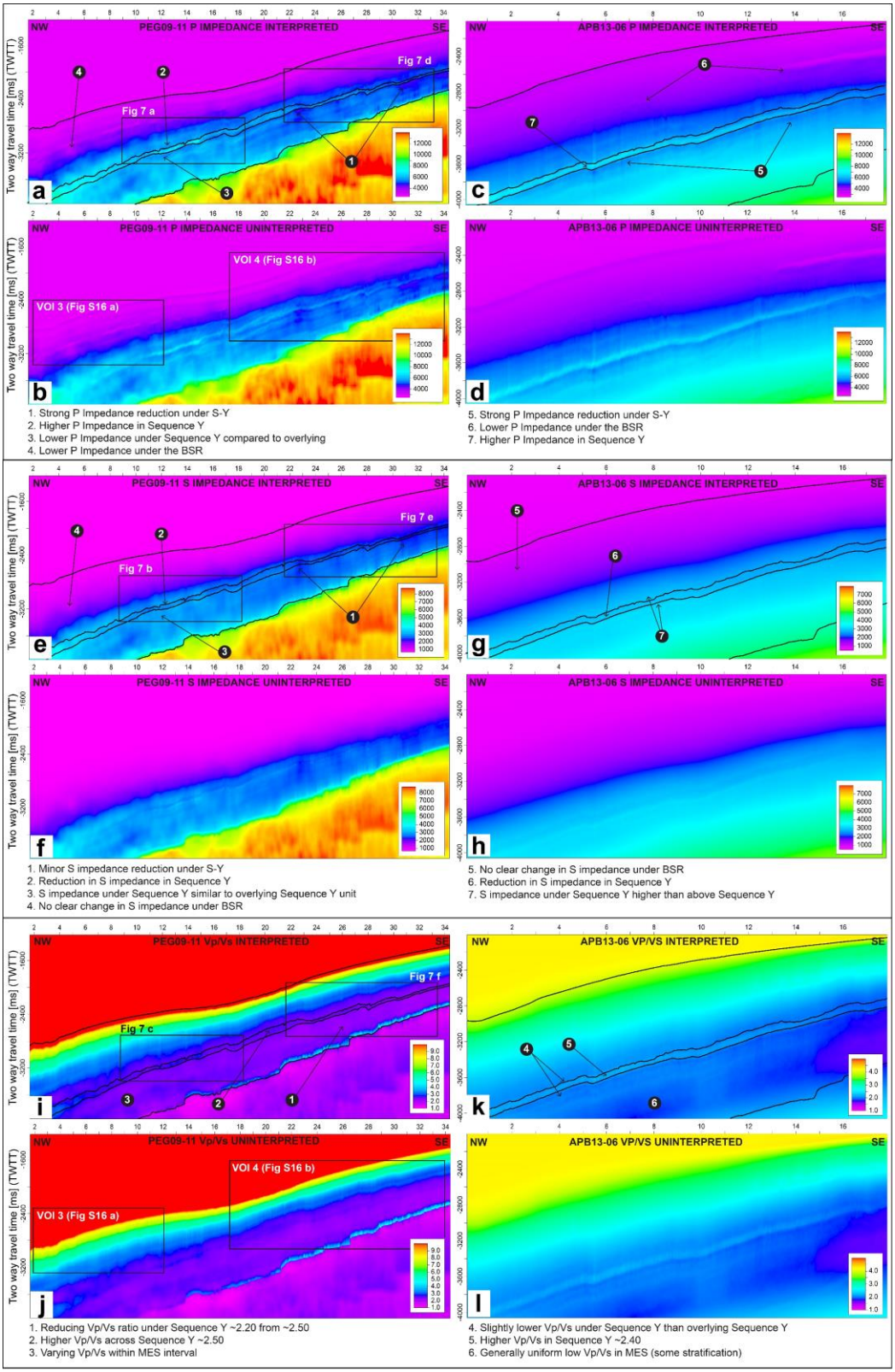
a
PEG09-11 P IMPEDANCE INTERPRETED
NW
SE
Fig 7 d
Fig 7 a
b
PEG09-11 P IMPEDANCE UNINTERPRETED
VOI 4 (Fig S16 b)
VOI 3 (Fig S16 a)
c
APB13-06 P IMPEDANCE INTERPRETED
d
APB13-06 P IMPEDANCE UNINTERPRETED
Two way travel time [ms] (TWTT)
1. Strong P Impedance reduction under S-Y
2. Higher P Impedance in Sequence Y
3. Lower P Impedance under Sequence Y compared to overlying
4. Lower P Impedance under the BSR
5. Strong P Impedance reduction under S-Y
6. Lower P Impedance under the BSR
7. Higher P Impedance in Sequence Y
e
PEG09-11 S IMPEDANCE INTERPRETED
Fig 7 e
Fig 7 b
f
PEG09-11 S IMPEDANCE UNINTERPRETED
g
APB13-06 S IMPEDANCE INTERPRETED
h
APB13-06 S IMPEDANCE UNINTERPRETED
1. Minor S impedance reduction under S-Y
2. Reduction in S impedance in Sequence Y
3. S impedance under Sequence Y similar to overlying Sequence Y unit
4. No clear change in S impedance under BSR
5. No clear change in S impedance under BSR
6. Reduction in S impedance in Sequence Y
7. S impedance under Sequence Y higher than above Sequence Y
i
PEG09-11 Vp/Vs INTERPRETED
Fig 7 f
Fig 7 c
j
PEG09-11 Vp/Vs UNINTERPRETED
VOI 4 (Fig S16 b)
VOI 3 (Fig S16 a)
k
APB13-06 VP/VS INTERPRETED
l
APB13-06 VP/VS UNINTERPRETED
1. Reducing Vp/Vs ratio under Sequence Y ~2.20 from ~2.50
2. Higher Vp/Vs across Sequence Y ~2.50
3. Varying Vp/Vs within MES interval
4. Slightly lower Vp/Vs under Sequence Y than overlying Sequence Y
5. Higher Vp/Vs in Sequence Y ~2.40
6. Generally uniform low Vp/Vs in MES (some stratification)

Figure S18. *(previous page) (a) PEG09-11 P-impedance interpreted. Inset black polygons shown in Figure 7. (b) PEG09-11 P-impedance uninterpreted. (c). APB13-06 P-impedance interpreted. (d) APB13-06 P-impedance uninterpreted. (e) PEG09-11 S-impedance interpreted. Inset black polygons shown in Figure 7. (f) PEG09-11 S-impedance uninterpreted. (g). APB13-06 S-impedance interpreted. (h) APB13-06 S-impedance uninterpreted. (i) PEG09-11 Vp/Vs ratios interpreted. Inset black polygons shown in Figure 7. (j) PEG09-11 Vp/Vs ratios uninterpreted. (k). APB13-06 Vp/Vs ratios interpreted. (l) APB13-06 Vp/Vs ratios uninterpreted. All P- and S-impedance measured in kPa.s/m.*

Text S10.

Figure 2 within the study shows some intersecting seismic lines appearing mismatched in amplitude values. Mismatch occurs between absolute amplitudes (e.g., dark blue intersecting white), and mismatch between polarity (e.g., red intersecting blue). Figure S19 shows how mismatch in amplitudes is an artefact of Petrel^{TM}'s voxel-based display of amplitudes. Voxels are densely-spaced at distant zoom, thus individual, small-scale changes in amplitude are difficult to resolve. As voxels remain constantly scaled independent of zoom, interference of larger-scale trends reduces the ability of the viewer to discern changes in amplitude, particularly at intersecting lines. We show 4 examples of this voxel-based display artefact. Mismatch of the degree of amplitude (e.g., APB13-28) is shown as incorrect when zoomed in (Figure S19). Mismatch of AVO polarity at intersections (e.g., APB13-06–PEG09-10) is similarly resolved as a scale artefact when zoomed upon (Figure S19).

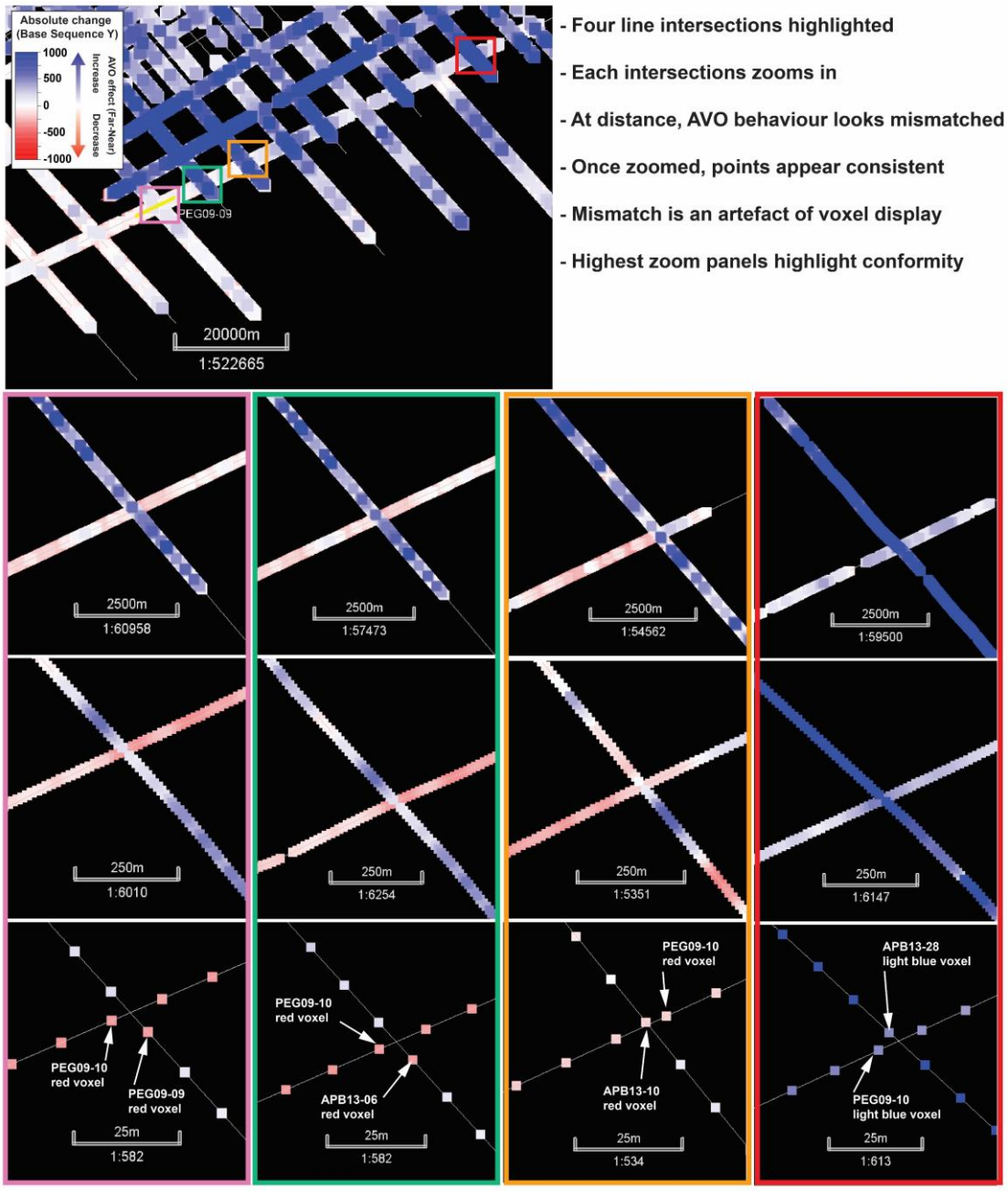

Figure S19. *(Top) Map of the study area showing the difference in amplitude between far and near angle stacks. Zoomed version of Figure 2. (Bottom). Mismatch between intersecting lines is common. Four mismatched amplitudes are highlighted as examples. Four coloured*

examples are progressively zoomed below the map. At the highest zoom (bottom windows), individual amplitude voxels are shown conforming between inline and crosslines.

Text S11. I show the pseudo borehole PEG01 within Figure S20. Here, the borehole was used to sample interval velocity at a 1-meter resolution, to produce a sonic log. Vs was estimated from this log using the Castagna et al. (1985) mudrock equation. I depict the PEG01 Vp log with depth in Figure 2.16 (middle window). Overlain is the U1520C Vp log for reference.

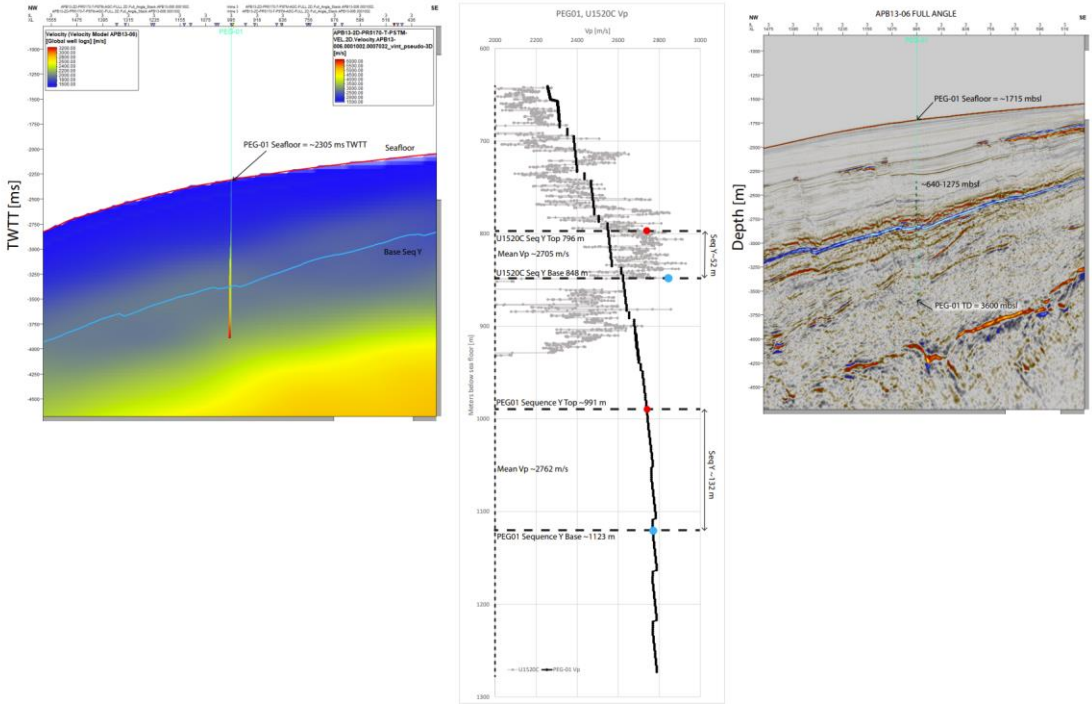

Figure S20. *(Left) APB13-06 interval velocity. Overlain, the pseudo borehole on the Chatham Rise northwestern slope (CRNWS) labelled PEG01. The Base Sequence Y and seafloor horizons shown. (Middle) Vp log from PEG09 with depth (m) in black. The U1520C Vp log (Wallace et al., 2019) is overlain for reference in grey, with two interpreted depths for Sequence Y. The Mesozoic sedimentary sequence (MES) is not encountered by U1520C. Red circles mark top and blue circles mark the base of Sequence Y respectively. (Right) APB13-06 full-angle section in depth (m). The seafloor is ~1715 m depth (~2300 ms TWTT), and the*

top of Sequence Y is ~991 meters below the seafloor (mbsf). Within U1520C, the top of Sequence Y is encountered at ~796 mbsf, ~200 meters shallower than the CRNWS.